Dalton Transactions

ROYAL SOCIETY OF CHEMISTRY

PAPER

View Article Online
View Journal | View Issue

Cite this: *Dalton Trans.*, 2024, **53**, 18183

The first example of polymeric lanthanide *tetrakis*-trifluoroacetates in chemical solution deposition of up-converting $NaGdF_4$:Yb,Er,Nd thin films†

Maria Burlakova, [a] Daria Blinnikova,[b] Gleb Volkonovskiy,[a] Haoyang Chai,[b,c] Dimitry Grebenyuk [a,c] and Dmitry Tsymbarenko *[a]

Received 15th April 2024,
Accepted 9th October 2024

DOI: 10.1039/d4dt01114g

rsc.li/dalton

A series of lanthanide *tetrakis*-trifluoroacetates $\{(detaH_2)_2[La_2(tfa)_8]_2(CH_3CN)_5(H_2O)_2\}_n$ and $(detaH_2)_n[Ln(tfa)_4]_{2n}$ (Ln = Pr–Eu), mixed-ligand complexes $[La(tfa)_3(CH_3CN)(H_2O)]_n$, $[Gd(tfa)_3(deta)_2]({}^{i}PrOH)$ and $[Yb(tfa)_2(deta)_2](tfa)$, as well as $detaH_2(tfa)_2$ were isolated and characterized. All lanthanide *tetrakis*-trifluoroacetates contain two types of 1D anionic chains $[Ln(tfa)_4]_n^{n-}$ and cavities occupied by $detaH_2^{2+}$ cations and solvating H_2O and CH_3CN molecules. The thermal behavior of $(detaH_2)_n[Ln(tfa)_4]_{2n}$ in air is investigated by TGA, *in situ* VT-PXRD and total X-ray scattering with PDF analysis, and the formation of metal fluorides occurs upon heating to 300 °C. The application of solution with lanthanide trifluoroacetates and diethylenetriamine (deta) as precursors for chemical deposition of β-$NaGdF_4$:Er,Yb,Nd thin films is reported. The deposited β-$NaGdF_4$:Er,Yb,Nd thin film demonstrates up-conversion luminescence under 980 and 808 nm laser excitation.

Introduction

Polymeric and polynuclear carboxylate complexes of rare-earth elements (REEs) are promising compounds to produce luminescent materials,[1–3] catalysts,[4–6] single molecular magnets,[7,8] and magnetocaloric materials.[9–11] REE ions possess similar coordination environments and chemical properties but differ in their electronic structures. Therefore, the presence of different REE cations with suitable *resonance energy levels* within one compound provides the possibilities for design of new luminescent thermometers,[1] sensors,[2,3] and up-conversion materials[12–15] due to the energy transfer between REE centers. Molecular clusters of lanthanides are also considered as secondary structural blocks for new coordination polymers of different dimensionalities from 1D chains to 3D frameworks.[16–21]

Thin films of hexagonal β-$NaLnF_4$ doped with Er^{3+}, Yb^{3+}, Tm^{3+}, Tb^{3+} or Nd^{3+} are considered as promising up-conversion materials because of low lattice phonon energies and crystal field strength for host materials based on β-$NaLnF_4$.[22–27] Up-conversion luminescent materials require a host material doped with at least two active elements (dual-doped system) – sensitizer and activator, *e.g.*, $NaY_{0.78}Yb_{0.20}Er_{0.02}$ and $NaY_{0.795}Yb_{0.20}Tm_{0.005}$.[28,29] More complicated systems, such as tri-doped β-$NaLnF_4$:Er,Yb,Nd, can demonstrate more effective luminescence.[30–34] For up-converting β-$NaLnF_4$:Yb,Er,Nd nanoparticles, the dopant content of 5% Nd, 2% Er and 20% Yb is often used[34–36] but at the same time, there are no reports in the literature regarding the optimal composition for β-$NaGdF_4$:Er,Yb,Nd thin films, as only β-$NaYF_4$:Nd films were obtained earlier.[37]

In any case, uniform distribution of elements is essential for multi-component $NaLnF_4$-based materials. The metal–organic chemical solution deposition (MOCSD) process allows both the precise control of cation composition and their uniform distribution. Fluorinated carboxylate complexes are possible molecular precursors for oxide and fluoride thin film materials in the MOCSD process.[38–40] One of its requirements is the precursor solution which does not crystallize upon solvent evaporation. Studies of precursor solution chemistry demonstrate that this can be achieved by hydrolysis[41–48] or polymerization of metal complexes.[49] The simultaneous coexistence of hydrolyzed and non-hydrolyzed forms for lanthanide cations in the gel is shown.

The hydrolysis additionally decreases the decomposition temperature of the precursor in the deposition of oxide thin films,[50] but for fluoride films thermal decomposition of intermediate hydroxocomplexes can result in the formation of oxy-

[a]*Department of Chemistry, Lomonosov Moscow State University, Moscow 119991, Russia. E-mail: tsymbarenko@gmail.com, tsymbarenko@inorg.chem.msu.ru*
[b]*Faculty of Materials Science, Lomonosov Moscow State University, Moscow 119991, Russia*
[c]*Faculty of Materials Science, MSU-BIT University, Shenzhen 518172, China*

†Electronic supplementary information (ESI) available: Crystallographic data details; supplementary tables and figures; XRD, TGA, EDX and AFM data. CCDC 2347608–2347614. For ESI and crystallographic data in CIF or other electronic format see DOI: https://doi.org/10.1039/d4dt01114g

carbonates and other by-products that complicates the deposition of a phase-pure material.[47]

Another way to control the nuclearity of complexes is using polydentate organic ligands. Generally, their addition leads to the formation of mono- or binuclear non-hydrolyzed isolated complexes[51–53] or coordination polymers.[54,55] Solutions of fluorinated complexes $[Ln_2(tfa)_6(diglyme)_2]$,[29] $[Ln(tfa)_2(deta)_2](tfa)$ (deta = diethylenetriamine),[51] $[Ln_2(pfp)_6Q_n]$ (Q = H_2O, diglyme),[56] or polymeric $[NaLn(tfa)_4(diglyme)]$,[57,58] $[NaY(tfa)_4(diglyme)]$, $[[Na(triglyme)_2][Y_2(tfa)_7(THF)_2]]$, and $[Na_2Y(tfa)_5(tetraglyme)]$[58] were previously exploited as precursors for the β-$NaLnF_4$ phase; however only a few examples of lanthanide *tetrakis*-trifluoroacetate systems were described.[38,39,59–62]

In this paper, we present the systematic study of complex formation in the $Ln(tfa)_3$–deta solution system and its application as a precursor for MOCSD of thin films.

Tetrakis-trifluoroacetates with Ln^{3+} (Ln = La–Eu) and protonated deta cations were observed for the first time. The crystal structures of polymeric $\{(detaH_2)_2[La_2(tfa)_8]_2(CH_3CN)_5(H_2O)_2\}_n$, $(detaH_2)_n[Ln(tfa)_4]_{2n}$ (Ln = Pr, Nd) and $[La(tfa)_3(CH_3CN)(H_2O)]_n$, as well as mononuclear mixed-ligand complexes $[Gd(tfa)_3(deta)_2]$(i-PrOH) and $[Yb(tfa)_2(deta)_2](tfa)$ were determined. The simultaneous coexistence of hydrolyzed and non-hydrolyzed forms for lanthanide cations in the gel is shown. The thin films of β-$NaGdF_4$:Er,Yb,Nd with up-conversion luminescence properties were prepared for the first time by MOCSD from the solution of lanthanide and sodium trifluoroacetates and diethylenetriamine.

Experimental

Materials and methods

Rare earth and sodium carbonates (analytical grade, Reakhim, Russia), trifluoroacetic acid (Htfa, 98%, P&M Invest, Russia), diethylenetriamine (deta, 99%, Sigma-Aldrich), (±)-3,7-dimethyl-1,6-octadien-3-ol (linalool, 97%, Düllberg Konzentra, Germany), diethyl ether (Medhimprom, Russia), acetonitrile and isopropanol (99%, Irea2000, Russia) were used as received. Na(tfa) and $Ln(tfa)_3(H_2O)_3$ were prepared from the corresponding metal carbonates and Htfa as reported earlier[45] and certified by TGA and PXRD.

The Ln content was determined by gravimetric analysis. TG-DTA data were obtained on a Derivatograph Q-1500 D in static air with a heating rate of 10 °C min^{-1} using an alumina crucible without a cap; the mass of the sample was 50 mg. FTIR spectra were recorded on a PerkinElmer Spectrum 3 FTIR spectrometer in attenuated total reflectance (ATR) geometry in the range of wavenumbers of 520–4000 cm^{-1}.

PXRD patterns at room temperature were recorded on a Rigaku MiniFlex 600 diffractometer (CuKα radiation, Kβ filter, D/teX Ultra detector) in the Bragg–Brentano geometry. Variable-temperature PXRD (VT-PXRD) experiments were performed in the temperature range 30–330 °C in the Debye–Scherrer geometry (2θ range 2.6–41.2°) on a Bruker D8 QUEST diffractometer (Photon III CMOS area detector, MoKα radiation, Montel optics) equipped with a hot air blower. Samples were placed into opened Kapton® capillaries of 0.5 mm diameter. *In situ* heating experiment was performed in a stepwise heating mode (10 °C per step) with the average heating rate of 2.5 °C min^{-1}. 2D diffraction patterns were processed using FormagiX software[63] and calibrated with a NIST SRM660c LaB_6 reference sample, as described recently.[46]

Total X-ray scattering data for pair distribution function (PDF) analysis were collected at room temperature for powder samples in Kapton® capillaries using the Bruker D8 QUEST diffractometer in the Q range of 0.3–17 $Å^{-1}$ as described recently.[46] PDF calculations were done with PDFgetX3 [64] using the data in the Q-range of 0.3 to 12.0 $Å^{-1}$; the refinements were carried out with DiffPy-CMI.[65] Atomic coordinates were taken from the crystal structure $(detaH_2)_n[Pr(tfa)_4]_{2n}$ and were fixed during the fit. The scale factor and quadratic peak broadening parameter have been refined.

XRD data for thin films were recorded in Bragg–Brentano geometry and grazing incidence geometry using Tongda TD-3700 (CuKα radiation, parabolic Göbel mirror, scintillator counter) and Rigaku MiniFlex 600 diffractometers.

Quantitative analysis of the film composition was performed by energy dispersive X-ray (EDX) spectroscopy using a Silicon Drift Detector X-Max with an active area of 80 mm^2 (Oxford Instruments), integrated into the Supra 50 VP (Leo) scanning electron microscope. The film was covered by a carbon layer prior to analysis to avoid the charging effect.

Atomic force microscopy (AFM) was performed using an NT-MDT NTEGRA Aura microscope operated in semi-contact mode. Up-conversion luminescence (UCL) spectra were recorded at room temperature using the setup based on an Ocean Optics USB2000 fiber-optic spectrometer and two diode lasers with an emission wavelength of 980 and 808 nm both with a pumping power of 800 mW (Besram Technology Inc., China).

Preparation of $\{(detaH_2)_2[La_2(tfa)_8]_2(CH_3CN)_5(H_2O)_2\}_n$ (1), $(detaH_2)_n[Ln(tfa)_4]_{2n}$, Ln = Pr (2), Nd (3), Sm (4), and Eu (5), and $[La(tfa)_3(CH_3CN)(H_2O)]_n$ (6)

Powder of $Ln(tfa)_3(H_2O)_3$ (28 mmol) was dissolved in 15–20 ml of acetonitrile at room temperature; then, deta (5.6 mmol) was added dropwise to the solution under vigorous stirring. The solution was left to complete evaporation of the solvent for 5–7 days. After 2 days, several colourless crystals of X-ray quality were obtained for **1** and **6**. The resulted residue was rinsed with diethyl ether and linalool to separate the crystalline precipitate from the gel-like by-product. The resulted precipitates consist mainly of $(detaH_2)_n[Ln(tfa)_4]_{2n}$ (Ln = Pr–Sm, **2–4**), while for Ln = Eu the phase **5** was observed predominately as a by-product (Fig. S1†). The yield was 20–40%.

Anal. calc. for $C_{20}H_{15}F_{24}N_3O_{16}Pr_2$ (**2**) (%): Pr, 21.83. Found (%): Pr, 22.87. FTIR (ν, cm^{-1}): 3295 (VW), 3088 (VW), 2972 (VW), 2934 (VW), 1804 (VW), 1734 (M), 1667 (S), 1640 (S),1620 (S), 1524 (W), 1488 (W), 1463 (M), 1419 (VW), 1387 (VW), 1350 (VW), 1317 (VW), 1193 (VS), 1169 (S), 1138 (VS), 1077 (M), 1044 (W), 1025 (W), 1010 (W), 969 (VW), 930 (VW), 902 (VW), 895

(VW), 857 (M), 841 (M), 795 (S), 747 (W), 729 (M), 718 (S), 681 (W), 606 (W).

Anal. calc. for $C_{20}H_{15}F_{24}N_3O_{16}Nd_2$ (**3**) (%): Nd, 22.23. Found (%): Nd, 22.09. FTIR (ν, cm^{-1}): 3295 (VW), 3083 (VW), 2976 (VW), 1802 (VW), 1791 (VW), 1737 (M), 1670 (S), 1642 (S), 1619 (M), 1524 (W), 1487 (W), 1463 (M), 1387 (VW), 1350 (VW), 1195 (VS), 1170 (S), 1140 (VS), 1077 (W), 1044 (VW), 1026 (VW), 1010 (VW), 970 (VW), 857 (M), 842 (M), 795 (S), 748 (W), 736 (M), 730 (M), 719 (S), 685 (VW), 607 (W).

Anal. calc. for $C_{20}H_{15}F_{24}N_3O_{16}Sm_2$ (**4**) (%): Sm, 22.96. Found (%): Sm, 23.16 FTIR (ν, cm^{-1}): 3298 (VW), 3082 (VW), 1804 (VW), 1742 (M), 1672 (S), 1643 (S), 1619 (M), 1523 (W), 1486 (W), 1464 (M), 1388 (VW), 1350 (VW), 1316 (VW), 1196 (VS), 1169 (S), 1140 (VS), 1077 (W), 1044 (W), 1026 (W), 1009 (W), 969 (W), 857 (M), 842 (M), 795 (S), 749 (W), 737 (M), 730 (M), 719 (S), 608 (W), 522 (M).

Anal. calc. for $C_{20}H_{15}F_{24}N_3O_{16}Eu_2$ (**5**) (%): Eu, 23.14. Found (%): Eu, 23.38. FTIR (ν, cm^{-1}): 3299 (W), 3083 (W), 3070 (W), 1807 (VW), 1746 (M), 1675 (S), 1646 (S), 1620 (M), 1522 (W), 1485 (W), 1467 (M), 1404 (W), 1368 (VW), 1349 (W), 1329 (W), 1306 (W), 1267 (W), 1196 (VS), 1171 (S), 1141 (VS), 1078 (W), 1058 (W), 1045 (W), 1025 (W), 1013 (W), 993 (W), 974 (W), 937 (VW), 858 (M), 842 (M), 829 (W), 795 (S), 780 (W), 749 (W), 737 (M), 729 (M), 719 (S), 690 (W), 669 (W), 649 (W), 608 (W), 522 (M).

Preparation of $[Gd(tfa)_3(deta)_2](iPrOH)$ (7) and $[Yb(tfa)_2(deta)_2](tfa)$ (8)

Powder of $Ln(tfa)_3(H_2O)_3$ (0.75 mmol) was dissolved in 2 mL of isopropyl alcohol (for **7**) or acetonitrile (for **8**); then, deta (1.5 mmol) was added dropwise to the solution under vigorous stirring. The mixture was left in an open vessel for slow evaporation. After 2 days, several colorless crystals of X-ray quality were obtained for **7** and **8**.

Preparation of $detaH_2(tfa)_2$ (9)

The solution of Htfa (12 mmol) in 5 mL of acetonitrile was added to the solution of deta (6 mmol) in 5 mL of acetonitrile, and the resulted solution was evaporated on a rotary evaporator to a residual volume of 5 mL. The crystalline precipitate was filtered and dried in air. The yield was 70%.

FTIR (ν, cm^{-1}): 3353 (VW), 3326 (VW), 3292 (VW), 3088 (M), 2952 (M), 2920 (M), 2868 (W), 2184 (VW), 2164 (VW), 2160 (VW), 1800 (VW), 1678 (S), 1594 (S), 1518 (M), 1470 (M), 1430 (M), 1386 (W), 1377 (W), 1361 (W), 1348 (W), 1319 (W), 1279 (W), 1172 (S), 1120 (VS).

X-ray crystallography

Single crystal X-ray diffraction data were collected on a Bruker D8 QUEST (50 kV, 1.4 mA, MoKα radiation, Montel optics, a Photon III CMOS area detector) at 100 K and on a Bruker APEX II (50 kV, 30 mA, MoKα radiation, a graphite monochromator, a CCD area detector). The data acquisition for weak needle-like crystals **1–3** was performed at an exposition time of 60–90 seconds per frame and these crystals demonstrated radiation damage and rapid decay of intensity of higher-angle peaks. The crystals were selected using a polarization microscope and then screened on a diffractometer. Crystals of **2**, **3**, **6**, and **9** were treated as single crystals, while other ones were treated as twins: **1** was refined as a two-component inversion twin; pseudo-merohedral twin **7** was de-twinned using the TwinRotMat algorithm as implemented in PLATON;[66] **8** was treated as a merohedral twin with a twin law (−1 0 0 0 −1 0 0 0 1).

The data were corrected for absorption by SADABS.[67] Crystal structures were solved by direct methods (SHELXS) or dual-intrinsic phasing (SHELXT) methods and refined anisotropically for all non-H atoms with the full-matrix F^2 least-squares technique (SHELXTL PLUS).[68–70] For structures **1**, **3**, **7**, the soft restrains on some C–F, C–C, and C–N bond distances and F–C–F, C–C–F angles were applied. All H atoms were placed in geometrically calculated positions and were refined in a riding mode. In structure **7**, the disordered iPrOH molecule was localized from Fourier synthesis but its refinement was unstable and resulted in a poor data-to-parameter ratio, thus it was finally excluded from refinement by the Squeeze procedure of PLATON.[67] Details of the data collection and refinement parameters are listed in Table S1, Fig. S2 and S3.†

Coordination polyhedra of the Ln atoms were determined using the continuous shape measures (CShM) approach as implemented in SHAPE2.1 software;[71] the results for **1–3**, **6–8** are listed in Tables S2–S6.†

Hirshfeld surface analysis for **1** and **3** was performed using CrystalExplorer software.[72]

Preparation of $NaGdF_4$:Yb,Er,Nd thin films

The precursor solutions for thin film deposition were prepared by dissolving metal trifluoroacetates in isopropyl alcohol. Powders of Na(tfa) (1.500 mmol), $Gd(tfa)_3(H_2O)_3$ (1.095 mmol), $Yb(tfa)_3(H_2O)_3$ (0.300 mmol), $Er(tfa)_3(H_2O)_3$ (0.030 mmol) and $Nd(tfa)_3(H_2O)_3$ (0.075 mmol) were dissolved in 5 mL of iPrOH at room temperature; then, deta (1.500 mmol) was added dropwise to the solution under vigorous stirring. Metal carboxylate films were deposited on a single-crystalline α-Al_2O_3 substrate of *C*-plane orientation employing the dip-coating technique with a pulling rate of 1 mm s^{-1} and a drying temperature of 150 °C. Then, the resulting amorphous precursor films were annealed at 600 °C for 15 min under argon with minor amounts of HF released from KHF_2.[56]

Results and discussion

Synthesis

The method of self-controlled hydrolysis is used for the reproducible synthesis of various lanthanide hydroxocomplexes with a target structure. Addition of aliphatic amines (*e.g.* deta) to a solution of lanthanide carboxylates promotes partial hydrolysis and stabilizes the REE hydroxocomplexes with low nuclearity of the metal–oxygen core, *e.g.* $\{Ln_4(OH)_4\}$ or $\{Ln_6(OH)_8\}$.[45–48] In the present work, the reaction of Ln $(tfa)_3(H_2O)_3$ with the reduced amount of deta (molar ratio of Ln : deta = 1 : 0.2) was studied. As a result, a series of non-hydrolyzed crystalline compounds of **1–6** were isolated from

the gel-like matrix. The single crystals of **1**, **2–3**, **6** and crystalline powders of **2–5** were characterized by XRD (Fig. 1), TG-DTA and FTIR. It was found that compounds **1–5** of general formula $(detaH_2)[Ln(tfa)_4]_2(Solv)_x$ are lanthanide *tetrakis*-trifuoroacetates, where the molar ratio of tfa^- to Ln^{3+} is higher than in the initial $Ln(tfa)_3(H_2O)_3$. Thus, the formation of **1–5** most probably occurs along with partial hydrolysis which provides the excess of tfa^- in the solution according to eqn (1):

$$8\,Ln(tfa)_3 + 2\,deta + 4H_2O \rightarrow 4\,1/n[Ln(tfa)_4]_n^{n-} + \{Ln_4(OH)_4\}^{8+} + 2\,deta\,H_2^{2+} + 8\,tfa^- \quad (1)$$

Indeed, for Ln = Pr, Nd the powders of **2** and **3** contain a minor admixture of the other crystalline phase $[Ln_4(OH)_4(tfa)_8(H_2O)_4]_n$ related to $[Gd_4(OH)_4(CF_3COO)_8(H_2O)_4]\cdot 2.5H_2O$.[73] This phase will be reported later. In the case of Ln = Eu, compound **5** can be hardly obtained as a pure product and frequently appears as an admixture to $[Eu_4(OH)_4(tfa)_8(H_2O)_4]_n$, while for heavier Ln = Gd and Yb the single crystals of mixed ligand complexes $[Gd(tfa)_3(deta)_2]$ (iPrOH) (**7**) and $[Yb(tfa)_2(deta)_2](tfa)$ (**8**) can be isolated (discussed in section 2.5 and 2.6 of the ESI†). Nevertheless, the formation of $(detaH_2)_n[Ln_2(tfa)_8]_n$ compounds has been shown even for heavy REEs including Lu (Fig. S1†).

Crystal structure of $\{(detaH_2)_2[La_2(tfa)_8]_2\cdot 5CH_3CN\cdot 2H_2O\}_n$ (1)

The structure **1** consists of two anionic polymeric chains $[La_2(tfa)_8]_n^{2n-}$, each formed by pairs of La atoms (La1, La2, or La3, La4, respectively) combined by bridging tfa^- anions (Fig. 2a and c, S7†). Cationic species $detaH_2^{2+}$ and solvating CH_3CN and H_2O molecules are packed within the chain cavities.

Anionic chains demonstrate a roughly similar geometry but they remarkably differ in La–O interatomic distances. Within the first chain (Fig. 2a), atoms La1 and La2 with CN being equal to 8 are in a similar square antiprismatic environment (CShM = 0.206 and 0.173, respectively) (Table S2†). Namely,

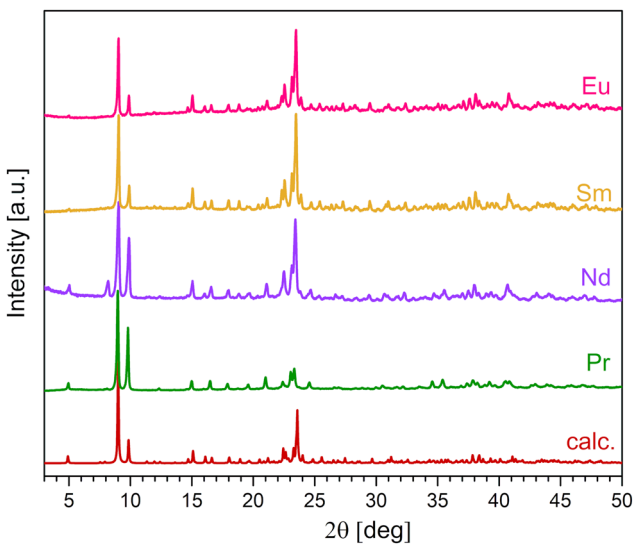

Fig. 1 PXRD data for powder samples of **2–5** (Pr–Eu), λ = 1.5418 Å.

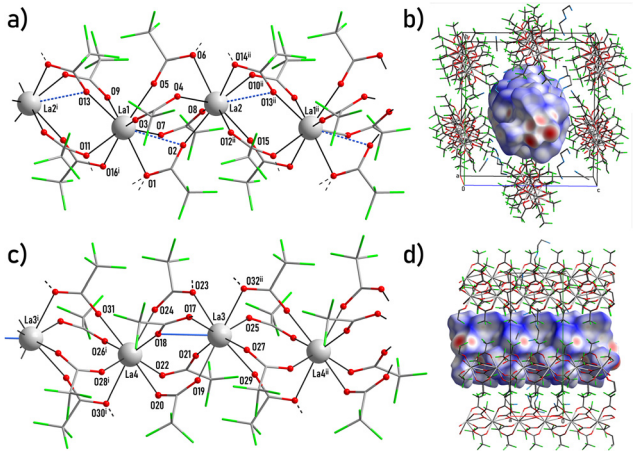

Fig. 2 Selected fragments of anionic chains of the first (a) and the second (c) types and their packing (b and d) in structure **1**. Hydrogen atoms are omitted for clarity. Black dashed lines show the directions of the hydrogen bonds. Blue lines show the elongated Ln–O contacts of chelate-bridging tfa^- ligands. A Hirshfeld surface decorated with the d_{norm} property is shown for the chain of the first type. Symmetry codes: (i) −1 + *x*, *y*, *z*, (ii) 1 + *x*, *y*, *z*, (iii) −*x*, −0.5 + *y*, −*z*, (iv) 1 − *x*, −0.5 + *y*, 1 − *z*.

La1 and La2 are coordinated by eight bridging carboxylate groups; the mean La–O distances are 2.532(13) Å and 2.529(18) Å respectively. Additionally, weak elongated contacts La1···O2 (3.033(17) Å) and La2···O13^{ii} (2.995(17) Å) reveal two carboxylate groups with slightly expressed chelate-bridging coordination (Table S8†). The scheme of both chains is shown in the ESI (Scheme 1†).

Within the second chain atoms La3 and La4 (Fig. 2c) possess different coordination environments. La3 is coordinated by seven bridging carboxylate groups (mean La3–O distance 2.502(13) Å) and one chelate-bridging carboxylate group. It is worth noting that the La3–O18 distance (2.882(17) Å, Table S7†) is only slightly longer than the typical La–O contact that allows one to consider it as a weak coordination bond. Therefore, the CN of La3 equals to 8 + 1 and the coordination polyhedron of La3 is best described as distorted muffin (CShM = 0.736, Table S2†). The La4 atom is coordinated by eight bridging carboxylate groups (mean La4–O distance 2.513(19) Å, Table S7†) with no chelate-bridging coordination. So, the CN of La4 equals to 8 and the coordination polyhedron of La4 is best described as square antiprism (CShM = 0.177, Table S2†).

The chains of both types are packed parallel to neighbours along the [100] direction. This packing can be virtually separated into alternating layers formed by the chains of one particular type. Therefore, chains form two-layered packing with a distorted 2D pseudo-hexagonal motif (Fig. S8†). The packing is loose and contains cavities occupied by $detaH_2^{2+}$ cations and solvating H_2O and CH_3CN molecules. Carboxylic groups of tfa^- anions, NH_3-groups of $detaH_2^{2+}$ cations and H_2O molecules form an extended framework of interchain hydrogen bonds (Table S8†) visualized as few isolated red-coloured d_{norm} spots on the chain side Hirshfeld surface (Fig. 2b and d).

Crystal structure of $(detaH_2)_n[Ln_2(tfa)_8]_n$, Ln = Pr(2), Nd(3), Sm(4), Eu(5)

According to single crystal XRD data for **2–3** and PXRD data for **2–5**, these compounds are isostructural and therefore only **3** will be discussed as an example.

The structure **3** consists of two different anionic polymeric chains $[Nd(tfa)_4]_n^{n-}$, each formed by certain type of Nd atoms (Nd1 or Nd2, respectively), and cationic species $detaH_2^{2+}$ (Fig. 3a and c, S9†). The coordination environment of Nd1 and Nd2 differs in detail despite the similar polyhedron (CN = 8, square antiprism, CShM = 1.312 and 0.044 respectively, Table S3†). Namely, Nd1 is coordinated by one chelating carboxylate group (Nd1–O1 and Nd1–O2 distances are 2.596(6) and 2.586(5) Å respectively) and six distinct bridging carboxylate groups (mean Nd1–O distance 2.45(3) Å). Nd2 is coordinated by the eight bridging carboxylate groups (mean Nd2–O distance 2.446(17) Å, Table S9†). The scheme of both chains is shown in the ESI (Scheme 2†).

The chains of both types are packed parallel to neighbors along the [001] direction. This structure can be considered as two-layered packing of chains (each layer is formed by the chains of only one type) with a distorted 2D pseudo-hexagonal motif (Fig. S10†). The packing is tighter than in that in the structure of **1** (as monitored by 2D lattice parameters ***u*** and ***v***, Table S9†) and the packing cavities are occupied only by $detaH_2^{2+}$ cations with no solvent molecules. Carboxylic groups of tfa^- anions and NH_3-groups of $detaH_2^{2+}$ cations form an extended framework of interchain hydrogen bonds (Table S10†) appeared as few isolated red-coloured d_{norm} spots on the chain side Hirshfeld surface (Fig. 3b and d). Nevertheless, according to Hirshfeld surface fingerprint analysis (Fig. S11†), O···H contacts make a minor contribution to intermolecular interactions (less than 13%), while F···F contacts predominate (with a contribution of 44–54%). This fact facilitates the preservation of the polymeric chain structure regardless of the removal of deta upon heating.

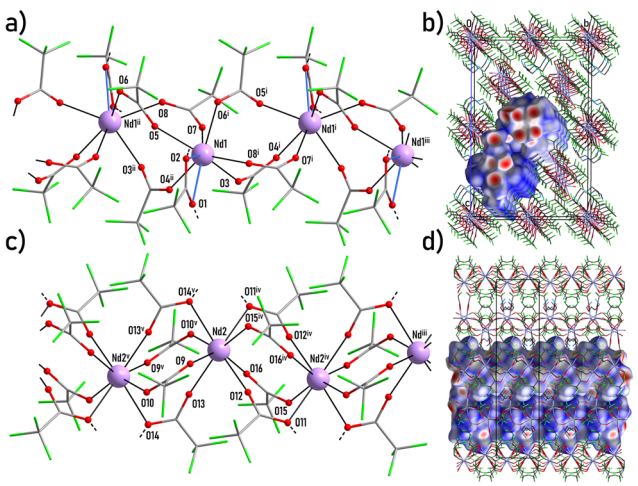

Fig. 3 Selected fragments of anionic chains of the first (a) and the second (c) types and their packing (b and d) in structure **3**. Hydrogen atoms are omitted for clarity. Black dashed lines show the directions of the hydrogen bonds. Blue lines show the Ln–O bonds of chelating tfa^- ligands. A Hirshfeld surface decorated with the d_{norm} property is shown for the chains of both types. Symmetry codes: (i) −0.5 + *x*, *y*, 0.5 − *z*, (ii) 0.5 + *x*, *y*, 0.5 − *z*, (iii) −1 + *x*, *y*, *z*, (iv) 2 − *x*, 1 − *y*, 1 − *z*, (v) 3 − *x*, 1 − *y*, 1 − *z*.

According to PXRD data, the unit cell parameters of **2–5** decrease along with reduction of ionic radius from Pr to Eu (Table S12†). More detailed description of structures **1–3** is presented in the ESI (sections 2.1–2.3†).

An overview of the structures **1** and **2–3** as well as PXRD data (Fig. 1, S1†) allows us to conclude that the anionic polymeric chains $[Ln(tfa)_4]_n^{n-}$ demonstrate high adjustability of the structure to the certain Ln due to variation of the coordination mode of the tfa^- ligand. Furthermore, the coordination number of 8 is appropriate for the entire REE series providing the existence of $[Ln(tfa)_4]_n^{n-}$ species for La–Lu. Some distinct examples of polymeric *tetrakis*-trifluoroacetates of light and heavy REEs[38–41] as well as binuclear fragments with similar four bridging tfa^- anions[29,74–76] confirm this concept. It is the existence of polymeric $[Ln(tfa)_4]_n^{n-}$ species for the entire REE series that facilitates the formation of mixed-metal polymers and allows us to obtain a homogeneous solution for the formation of $NaLnF_4$ films.

Thermal behavior of $(detaH_2)_n[Ln_2(tfa)_8]_n$, Ln = Pr(2), Nd(3), Sm(4), Eu(5)

Since $(detaH_2)_n[Ln_2(tfa)_8]_n$ compounds are present in the solution used to deposit fluoride thin films, a thorough study of their thermolysis is essential. The thermal behavior of **2–5** in air was investigated in the temperature range of 20–1000 °C by TGA (Fig. 4, left panel, Fig. S21–S24†) and additionally decomposition of **2** was monitored *in situ* by VT-PXRD in the temperature range of 30–330 °C (Fig. 4, right panel). Compounds **2–5** demonstrate similar thermal behavior with three stages of decomposition which are described for representative complex **2**. Firstly, a hardly resolved stage of minor weight loss (7.9%) in the 200–230 °C range is best attributed to elimination of deta (NB, b.p. of deta is 204–207 °C (ref. 77)) and formation of the intermediate phase $[HPr(tfa)_4]_n$ (calculated weight loss 8%). The elimination of deta affects the crystal structure of the coordination polymer to splitting of major peaks in the VT-PXRD pattern; however the product retains its overall crystallinity (Fig. 4, right panel). The second stage occurs in the 240–280 °C range and corresponds to the thermolysis of tfa^- and formation of PrF_3 as confirmed by PXRD (Fig. 4, right panel). It is worth noting that the heating of lanthanide carboxylates in the presence of amines can result in the formation of oxycarbonates instead of trifluorides.[28] Fortunately, this is not the case for compounds **2–5**, where deta molecules are located outside the robust $[Ln(tfa)_4]_n^{n-}$ polymeric chains and are removed from the compound prior to thermolysis. This behavior allows us to avoid the formation of undesirable products during the deposition of thin films. Finally, PrF_3 undergoes pyrohydrolysis above 600 °C, which is typical of REE trifluorides,[78,79] and transforms to the mixture of PrOF and PrO_x (*e.g.*, Pr_6O_{11}).

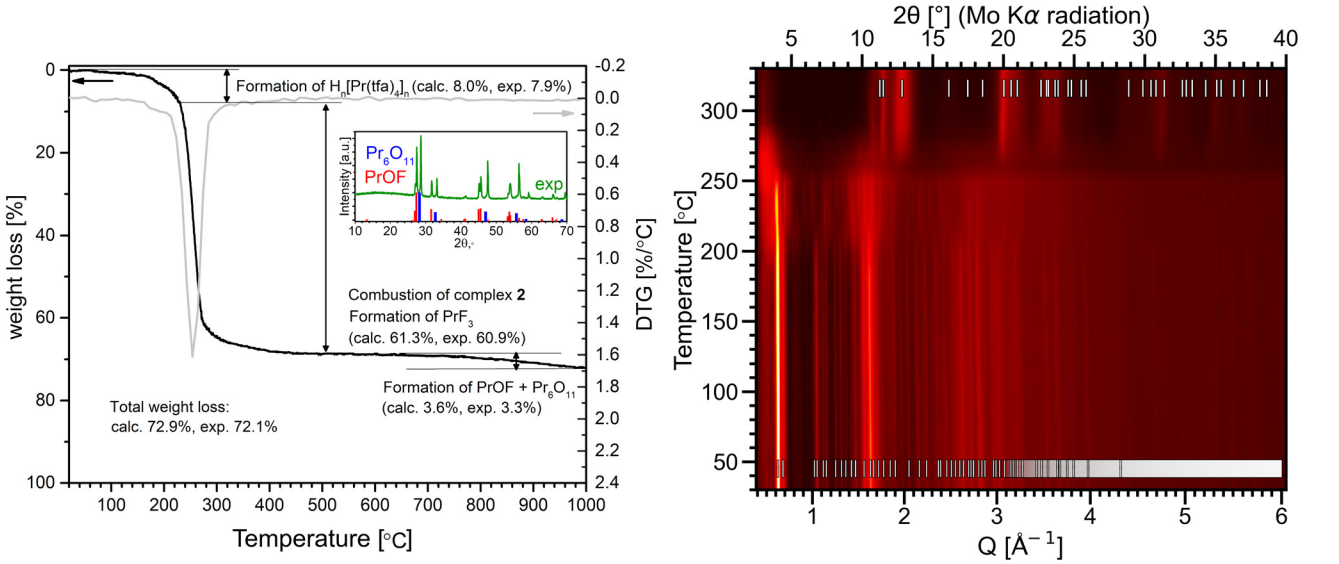

Fig. 4 The data of TGA (left) and VT-PXRD (right) on the thermal behavior of **2** upon heating in air. On the left, black line shows the TG curve, the pale grey line shows the DTG curve, the insert presents the PXRD of the residue compared to cards [44-1312] for PrOF and [42-1121] for Pr_6O_{11} from PDF-2 database, λ = 1.5418 Å. On the right, white vertical bars show the calculated positions of intense (>3%) PXRD peaks for $(detaH_2)_n[Pr(tfa)_4]_{2n}$ (down) and PrF_3 (up), λ = 0.7107 Å.

The structural features of **2** and the intermediate phase **2′**, obtained by heat-treatment of **2** at 230 °C followed by cooling to room temperature, were investigated by total X-ray scattering with Pair Distribution Function (PDF, $G(r)$) analysis (Fig. 5). Owing to the strong scattering power of Ln atoms, the most intense peaks in the $G(r)$ of the polymer $(detaH_2)_n[Pr_2(tfa)_8]_n$ originate from the closest Ln···O (at *ca.* 2.5 Å) and Ln···Ln (at *ca.* 3.5–5.0, 8.6–9.0 and 12.5–13.0 Å) contacts. The experimental $G(r)$ of intermediate phase **2′** after 230 °C differs slightly from $G(r)$ of **2** in the short range, 1–6.1 Å, and shows the noticeable decay in the mid-range, 6.1–25 Å. Nevertheless, the Pearson correlation coefficient, pcc = 0.916 for 1.0–10.0 Å and pcc = 0.688 for 10.0–25.0 Å, shows the similarity of $G(r)$ function for **2** before and after heating to 230 °C in the range which describes the local structure and closest interatomic contacts. Thus, one can suppose the preservation of the anionic chain $[Pr(tfa)_4]_n^{n-}$ motif after deta elimination, although the anionic chains become less regular.

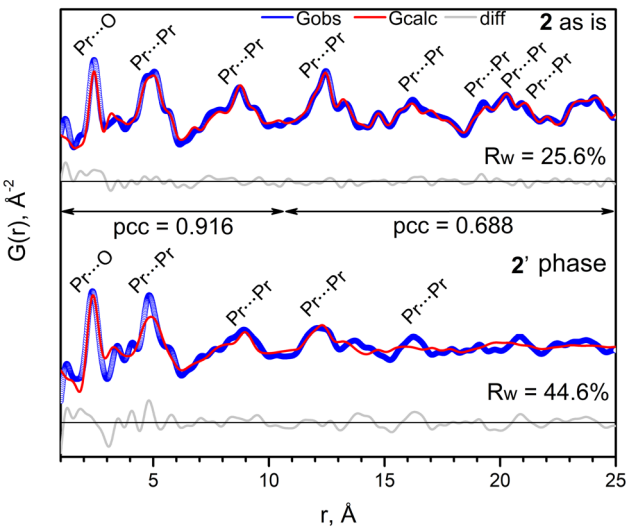

Fig. 5 The experimental PDF (Q_{max} = 12 Å^{-1}) of **2** and **2′** powders and fits by the model of the $(detaH_2)_n[Pr(tfa)_4]_{2n}$ crystal. Pearson correlation coefficients (pcc) for short- and mid-ranges compare experimental PDF of **2** and **2′**.

Deposition of β-$NaGdF_4$:Yb,Er,Nd film

Preparation of β-$NaGdF_4$:Yb,Er,Nd thin films was performed by MOCSD which provides the precise control of the complex cationic composition essential for up-conversion applications. The isopropanol solution of REE and sodium trifluoroacetates was used as a source of cations and fluorine atoms. Addition of an excess of deta modifies the viscosity of solution and prevents undesired crystallization of dissolved metal salts upon solvent evaporation due to *in situ* formation of polynuclear hydroxocomplexes with the $\{Ln_4(OH)_4\}$ core[46] and polymeric $[Ln(tfa)_4]_n^{n-}$ species similar to **1–5**. Moreover, the polymeric nature of **1–5** structures contributes to homogeneous distribution of different metal cations within the precursor solution.

Dip-coating of the c-Al_2O_3 substrate and further annealing at 600 °C resulted in the formation of the single-phase polycrystalline film of β-$NaGdF_4$:Yb,Er,Nd. Indeed, GIXRD data (Fig. 6) agree with the reference XRD pattern of hexagonal β-$NaGdF_4$, and minor peak shifts occur due to doping of the latter with a significant amount of smaller Yb^{3+} cations. θ–2θ XRD data contain the peaks corresponding to the β-$NaGdF_4$ without preferred orientation. The formation of the cubic α-$NaLnF_4$ phase was not observed due to the Gd-based matrix[27] and this is ben-

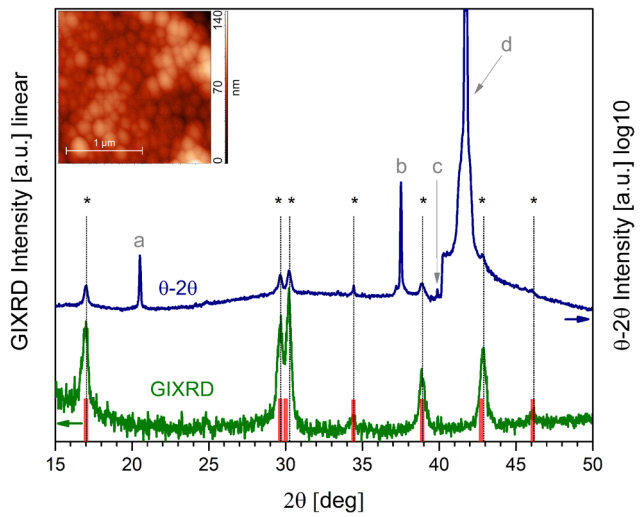

Fig. 6 θ–2θ and GIXRD patterns (ω = 0.5°) of thin films annealed at 600 °C. Lattice parameters: $a = b$ = 6.0281(8) Å, c = 3.5891(9) Å, $\alpha = \beta$ = 90°, γ = 120°, V = 112.95(2) Å^3. Reflections denoted as a–d, respectively, refer to (a) $\lambda/2$ reflections for c-Al_2O_3 (006), (b) CuK_β, (c) WK_α and (d) c-Al_2O_3 (006). Inset shows AFM height profiles of fluoride thin films.

eficial for the up-conversion efficiency.[80] The composition of the thin film monitored by EDX analysis shows a tailored cationic ratio (Fig. S25†).

According to the AFM study, the film has a folded surface formed by grains with a lateral size of 0.15–0.30 μm (Fig. 6, S26†).

Up-conversion luminescence of β-$NaGdF_4$:Yb,Er,Nd film

The β-$NaGdF_4$:Yb,Er,Nd film corresponds to a tri-doped system and contains Yb^{3+} and Nd^{3+} as sensitizers and Er^{3+} as the activator. In particular, Yb^{3+} absorbs near infrared (NIR) photons whose energy is close to the energy of the Yb:$|^2F_{7/2}\rangle \rightarrow |^2F_{5/2}\rangle$ transition, 10.2×10^3 cm^{-1} or λ_{max} = 976 nm; moreover, Yb^{3+} promotes transfer of energy to Er^{3+}. The presence of Nd^{3+} allows the absorption of NIR photons with a shorter wavelength due to the electron transition Nd:($|^4I_{9/2}\rangle \rightarrow |^4F_{5/2}\rangle$), 12.5×10^3 cm^{-1} or λ_{max} = 800 nm. As a result, the deposited film of β-$NaGdF_4$:Yb,Er,Nd demonstrates an intense eye-visible up-conversion luminescence under 980 and 808 nm laser excitation (Fig. 7) despite the small amount of luminophore within the film. The up-conversion luminescence spectra contain typical emission bands which correspond to electron transitions for the Er^{3+} (655, 540 and 525 nm: $|^4F_{9/2}\rangle \rightarrow |^4I1_{5/2}\rangle$; $|^2H_{11/2}\rangle \rightarrow |^4I_{15/2}\rangle$; $|^4S_{3/2}\rangle \rightarrow |^4I_{15/2}\rangle$, respectively) and agree with the emission spectrum of β-$NaGdF_4$:Yb,Er,Nd nanoparticles of similar composition.[34]

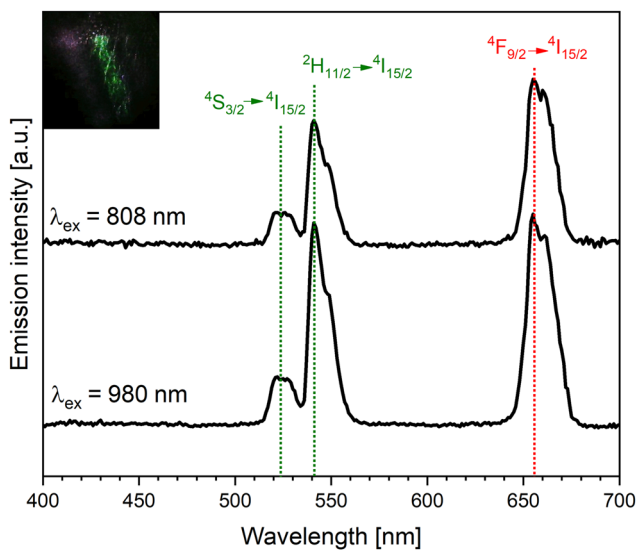

Fig. 7 The emission UCL spectra for thin film $NaGdF_4$:Yb,Er,Nd. The inset shows the photo of a green emission of up-converted radiation at λ_{ex} = 808 nm and a violet emission of scattered exciting radiation.

Conclusions

Nowadays, the chemical transformations of REE carboxylates, including trifluoroacetates, in the presence of amines are being actively studied. Mono- and binuclear mixed-ligand complexes, polynuclear hydroxocomplexes and hydroxogels are known as products of these transformations, reflecting the competition between complexation and hydrolysis processes. It is necessary to study the composition, structure and thermal behaviour of the compounds formed in this system to understand the mechanism of their transformation to the final material.

In the present work, the effect of diethylenetriamine (deta) on crystallization of lanthanide trifuoroactetates was studied. The crystalline lanthanide *tetrakis*-trifluoroacetates $[(detaH_2)[Ln_2(tfa)_8](Solv)_x]_n$ were revealed for the entire REE series (La–Lu) and isolated from the gel-matrix for Ln = La(**1**), Pr(**2**), Nd (**3**), Sm(**4**) and Eu(**5**) in the absence of deta, while the excess of deta leads to viscous homogeneous gel-like solutions stable towards spontaneous crystallization and suitable for preparation of inorganic materials.

The complexes for **1** and **2–5** have similar crystal structures and are formed from 1D polymer anionic chains $[Ln(tfa)_4]_n^{n-}$ arranged in a pseudohexagonal motif. The cavities between the chains contain $detaH_2^{2+}$ cations and solvent molecules. When heated in air, these complexes eliminate deta instead of hydrolysis, while the motif of the chains remains unaffected up to 260 °C when compounds transform to REE fluorides.

It is worth noting that the coordination environment of the Ln ion in $[(detaH_2)[Ln_2(tfa)_8](Solv)_x]_n$ polymers easily adapts to a specific REE, maintaining the structure of $[Ln(tfa)_4]_n^{n-}$ anionic chains and making accessible the combination of different REEs within each species in the precursor solution. One could expect that $detaH_2^{2+}$ cations which surround $[Ln(tfa)_4]_n^{n-}$ anionic species can be replaced by Na^+ cations in the precursor solution. These features contribute to the homogeneity of solution, prevent the precipitation of individual metal compounds during solvent evaporation and lead to the

formation of complex fluoride thin films at moderate temperature.

Thus, we have developed precursors that realize the advantages of deta amine (for control of viscosity and crystallization), but at the same time avoid the formation of LnO_xF_y phases unsuitable for up-conversion application.

The solution based on REE and sodium trifluoroacetates with deta was applied as a precursor for MOCSD preparation of the tri-doped β-$NaGdF_4$:Nd,Yb,Er film. Due to the simultaneous neodymium and ytterbium action as sensitizers, the film exhibits up-converting luminescence upon excitation at wavelengths of λ_{ex} = 808 nm and λ_{ex} = 980 nm. It is worth noting that the up-converting luminescence with λ_{ex} = 808 nm was observed for the first time for the film sample.

Author contributions

D. T. conceived the idea, secured funding, and supervised the project. M. B., G. V. and D. G. synthesized the compounds. M. B. characterized the products by FTIR, TGA and PXRD. D. T. collected and processed the single-crystal XRD data. D. T. and M. B. solved and refined the crystal structures. D. T. collected VT-PXRD and total X-ray scattering data for PDF analysis. D. T. and M. B. interpreted the data and refined the models. H. C. performed the Hirshfeld surface analysis. D. B. and M. B. deposited thin films and analysed the up-conversion spectra. D. T. characterized the films by AFM and XRD. M. B., D. G. and D. T. discussed the results. M. B. took the lead in writing of the manuscript with contributions from D. T., D. G. and D. B. All authors have given approval to the final version of the manuscript.

Data availability

Crystallographic data for compounds **1–3**, and **6–9** have been deposited at the CCDC under 2347608–2347614.† The XRD, TGA, EDX and AFM data supporting this article have been included as part of the ESI.† Data can be made available upon request.

Conflicts of interest

There are no conflicts to declare.

Acknowledgements

The authors acknowledge support from the M. V. Lomonosov Moscow State University Program of Development. Research was carried out under partial support of the MSU Shared Research Equipment Centre "Technologies for obtaining new nanostructured materials and their complex study", National Project "Science". This work has received funding from the Russian Science Foundation (Project No. 22-73-10089).

References

1 H. Yao, G. Calvez, C. Daiguebonne, K. Bernot, Y. Suffren and O. Guillou, *Inorg. Chem.*, 2019, **58**, 16180.
2 X. Zhou, H. Li, H. Xiao, L. Li, Q. Zhao, T. Yang, J. Zuo and W. Huang, *Dalton Trans.*, 2013, **42**, 5718.
3 Y. Cui, H. Xu, Y. Yue, Z. Guo, J. Yu, Z. Chen, J. Gao, Y. Yang, G. Qian and B. Chen, *J. Am. Chem. Soc.*, 2012, **134**, 3979.
4 M. Lammert, M. Wharmby, S. Smolders, B. Bueken, A. Lieb, K. Lomachenko, D. De Vos and N. Stock, *Chem. Commun.*, 2015, **51**, 12578.
5 C. Pagis, M. Ferbinteanu, G. Rothenberg and S. Tanase, *ACS Catal.*, 2016, **6**, 6063.
6 Y. Liu, K. Mo and Y. Cui, *Inorg. Chem.*, 2013, **52**, 10286.
7 J.-H. Jia, Q.-W. Li, Y.-C. Chen, J.-L. Liu and M.-L. Tong, *Coord. Chem. Rev.*, 2019, **378**, 365.
8 J.-J. Hu, Y. Peng, S.-J. Liu and H.-R. Wen, *Dalton Trans.*, 2021, **50**, 15473.
9 A. S. Dinca, A. Mindru, D. Dragancea, C. Tiseanu, S. Shova, S. Cornia, L. M. Carrella, E. Rentschler, M. Affronte and M. Andruh, *Dalton Trans.*, 2019, **48**, 1700.
10 F. S. Guo, J. D. Leng, J. L. Liu, Z. S. Meng and M. L. Tong, *Inorg. Chem.*, 2012, **51**, 405.
11 W.-M. Wang, X.-Z. Li, L. Zhang, J.-L. Chen, J.-H. Wang, Z.-L. Wu and J.-Z. Cui, *New J. Chem.*, 2019, **43**, 7419.
12 X.-Z. Li, C.-B. Tian and Q.-F. Sun, *Chem. Rev.*, 2022, **122**, 6374.
13 A. Nonat and L. Charbonnière, *Coord. Chem. Rev.*, 2020, **409**, 213192.
14 N. Souri, P. Tian, C. Platas-Iglesias, W. Ka-Leung, A. Nonat and L. Charbonnière, *J. Am. Chem. Soc.*, 2017, **139**, 1456.
15 L. Luo, W. P.-W. Lai, K.-L. Wong, W.-T. Wong, K.-F. Li and K.-W. Cheah, *Chem. Phys. Lett.*, 2004, **398**, 372.
16 L. Feng, J. Pang, P. She, J.-L. Li, J.-S. Qin, D.-Y. Du and H.-C. Zhou, *Adv. Mater.*, 2020, **32**, 202004414.
17 S. Ma, D. Yuan, X.-S. Wang and H.-C. Zhou, *Inorg. Chem.*, 2009, **48**, 2072.
18 D. Grebenyuk, M. Shaulskaya, A. Shevchenko, M. Zobel, M. Tedeeva, A. Kustov, I. Sadykov and D. Tsymbarenko, *ACS Omega*, 2023, **8**(50), 48394.
19 T. Gorai, W. Schmitt and T. Gunnlaugsson, *Dalton Trans.*, 2021, **50**, 770.
20 Y. Hasegawa and Y. Kitagawa, *J. Photochem. Photobiol., C*, 2022, **51**, 100485.
21 A. Kateshali, S. Dogaheh, J. Soleimannejad and A. Blake, *Coord. Chem. Rev.*, 2020, **419**, 213392.
22 T. Kano, H. Yamamoto and Y. Otomo, *J. Electrochem. Soc.*, 1972, **119**, 1561.
23 J. Yao, C. Huang, C. Liu and M. Yang, *Talanta*, 2020, **208**, 120157.
24 T. Q. H. Tran, M. H. Hoang, T. A. T. Do, A. T. Le, T. H. Nguyen, T. D. Nguyen and M. T. Man, *J. Lumin.*, 2021, **237**, 118162.
25 F. Wang and X. Liu, *Chem. Soc. Rev.*, 2009, **38**, 976.

26 P. Zhang, H. Chen, Y. Yang, D. Zhao, Z. Jia, K. Zheng, G. Qin and W. Qin, *J. Alloys Compd.*, 2018, **753**, 725.
27 B. Sobolev, in *Part 1. The High Temperature Chemistry of the Rare Earth Trifluorides//The Rare Earth Trifluorides*, Institut d'Estudis Catalans, 2000, p. 520.
28 N. Menyuk, K. Dwight and J. Pierce, *Appl. Phys. Lett.*, 1972, **21**, 159.
29 H. Ayadi, W. Fang, S. Mishra, E. Jeanneau, G. Ledoux, J. Zhang and S. Daniele, *RSC Adv.*, 2015, **5**, 100535.
30 S. T. Dibaba, X. Ge, W. Ren and L. Sun, *J. Rare Earths*, 2019, **37**, 791.
31 N. Song, S. Liu, P. Zhang, J. He, Q. Zhang, F. Wang and B. Zhou, *J. Rare Earths*, 2021, **39**, 1506.
32 Q. Su, H.-L. Wei, Y. Liu, C. Chen, M. Guan, S. Wang, Y. Su, H. Wang, Z. Chen and D. Jin, *Nat. Commun.*, 2021, **12**, 4367.
33 C. Li, X. Li and X. Liu, *ACS Appl. Mater. Interfaces*, 2022, **14**, 10947.
34 J. Shen, G. Chen, A.-M. Vu, W. Fan, O. S. Bilsel, C.-C. Chang and G. Han, *Adv. Opt. Mater.*, 2013, **1**, 644.
35 I. Mikalauskaite, G. Pleckaityte, L. Sinusaite, V. Plausinaitiene, A. Katelnikovas and A. Beganskiene, *J. Lumin.*, 2020, **223**, 117237.
36 X. Li, R. Wang, F. Zhang, L. Zhou, D. Shen, C. Yao and D. Zhao, *Sci. Rep.*, 2013, **3**, 3536.
37 J. Barranco, A. Méndez-Blas and M. Calixto, *J. Mater. Sci.: Mater. Electron.*, 2019, **30**, 4855.
38 S. Mishra and S. Daniele, *Chem. Rev.*, 2015, **115**(16), 8379.
39 T. Boyle, D. Yonemoto, J. Sears, L. Treadwell, N. Bell, R. Cramer, M. Neville, G. Stillman and S. Bingham, *Polyhedron*, 2017, **137**, 59.
40 S. Scharf, S. Notz, M. Abdeldayem, R. Thomas, M. Weber, M. Mehring, M. Franz, D. Rittrich, S. Schulz and H. Lang, *Mater. Chem. Phys.*, 2023, **301**, 127634.
41 J. Kobylarczyk, E. Kuzniak, M. Liberka, S. Chorazy, B. Sieklucka and R. Podgajny, *Coord. Chem.*, 2020, **419**, 213394.
42 H. Yao, G. Calvez, C. Daiguebonne, K. Bernot, Y. Suffren, M. Puget, C. Lescop and O. Guillou, *Inorg. Chem.*, 2017, **56**(23), 14632.
43 G. Giester, Z. Žák and P. Unfried, *J. Alloys Compd.*, 2009, **481**, 116.
44 V. Guillerm, Ł. Weseliński, Y. Belmabkhout, A. Cairns, V. D'Elia, Ł. Wojtas, K. Adil and M. Eddaoudi, *Nat. Chem.*, 2014, **6**, 673.
45 D. Grebenyuk, I. Martynova and D. Tsymbarenko, *Eur. J. Inorg. Chem.*, 2019, **26**, 3103.
46 D. Tsymbarenko, D. Grebenyuk, M. Burlakova and M. Zobel, *J. Appl. Crystallogr.*, 2022, **55**, 890.
47 M. Burlakova, M. Shaulskaya, A. Anosov and D. Tsymbarenko, *J. Struct. Chem.*, 2023, **64**, 112528.
48 D. Tsymbarenko, D. Grebenyuk, M. Burlakova and A. Shurkina, *Russ. J. Coord. Chem.*, 2022, **48**, 168.
49 T. Schneller, R. Waser, M. Kosec and D. Payne, in *Chemical Solution Deposition of Functional Oxide Thin Films*, Springer-Verlag Wien, 2013, p. 103.
50 S. Mishra, G. Ledoux, E. Jeanneau, S. Daniele and M.-F. Joubert, *Dalton Trans.*, 2012, **41**, 1490.
51 D. Grebenyuk, N. Ryzhkov and D. Tsymbarenko, *J. Fluor. Chem.*, 2017, **202**, 82.
52 T. Madanhire, H. Davids, M. C. Pereira, E. C. Hosten and A. Abrahams, *Polyhedron*, 2020, **185**, 114583.
53 A. Rohdea and W. Urland, *Dalton Trans.*, 2006, **24**, 2974.
54 M.-L. Chen, X. Tang, T.-H. Lu, X.-Q. Zhan and Z.-H. Zhou, *J. Coord. Chem.*, 2019, **72**, 1547.
55 H. Munasinghe, R. Szlag, M. Imer and F. Rabuffetti, *Inorg. Chem.*, 2022, **61**, 5588.
56 A. Shevchenko, A. Anosov, D. Blinnikova, D. Grebenyuk and D. Tsymbarenko, *Metals*, 2022, **12**, 488.
57 Y. Chen, S. Mishra, G. Ledoux, E. Jeanneau, M. Daniel, J. Zhang and S. Daniele, *Chem. – Asian J.*, 2014, **9**, 2415.
58 S. Mishra, S. Daniele, G. Ledoux, E. Jeanneau and M.-F. Joubert, *Chem. Commun.*, 2010, **46**, 3756.
59 D. John, A. Rohde and W. Urland, *Z. Naturforsch., B: J. Chem. Sci.*, 2006, **61**(6), 699.
60 Y. Haiyun, G. Calvez, C. Daiguebonne, K. Bernot, Y. Suffren and O. Guillou, *Inorg. Chem.*, 2019, **58**, 16180.
61 M. A. Mansoor, M. Mazhar, M. Ebadi, H. N. Ming, M. A. M. Teridi and L. K. Mun, *New J. Chem.*, 2016, **40**, 5177.
62 Y. Shen, G. Cosquer, B. K. Breedlove and M. Yamashita, *Magnetochemistry*, 2016, **2**, 44.
63 D. Tsymbarenko, FormagiX. 2D XRD Processing Software, **https://formagix.org/** (accessed 2023-12-21).
64 P. Juhás, T. Davis, C. Farrow and S. Billinge, *J. Appl. Crystallogr.*, 2013, **46**, 560.
65 P. Juhás, C. Farrow, X. Yang, K. Knox and S. Billinge, *Acta Crystallogr., Sect. A: Found. Adv.*, 2015, **71**, 562.
66 A. Spek, *Acta Crystallogr., Sect. E: Crystallogr. Commun.*, 2020, **76**, 1.
67 G. Sheldrick, *SADABS v.2.01, Bruker/Siemens Area Detector Absorption Correction Program*, Bruker AXS, Madison, Wisconsin, USA, 1998.
68 G. Sheldrick, SHELXTL – integrated space-group and crystal-structure determination, *Acta Crystallogr., Sect. A: Found. Adv.*, 2015, **71**, 3.
69 G. Sheldrick, Crystal structure refinement with SHELXL, *Acta Crystallogr., Sect. C: Struct. Chem.*, 2015, **71**, 3.
70 *Bruker. SHELXTL XT, Program for crystal structure solution, v. (2014)/4*, Bruker AXS Inc., Madison, WI, 2014.
71 D. Casanova, M. Llunell, P. Alemany and S. Alvarez, *Chem. – Eur. J.*, 2005, **11**(5), 1479.
72 P. Spackman, M. Turner, J. McKinnon, S. Wolff, D. Grimwood, D. Jayatilakab and M. Spackman, *J. Appl. Crystallogr.*, 2021, **54**, 1006.
73 D. John and W. Urland, *Z. Anorg. Allg. Chem.*, 2007, **633**, 2587.
74 S. Bone, D. Sowerby and R. Verma, *Dalton Trans.*, 1978, 1544.
75 N. Dong, H. Wang, R. Barton and B. Robertson, *J. Coord. Chem.*, 1990, **22**, 191.
76 P.-R. Wei, D.-D. Wu, Z.-Y. Zhou, S.-L. Li and T. C. W. Mak, *Polyhedron*, 1997, **16**, 749.

77 Aldrich Chemical Company Inc., *Catalog Handbook of Fine Chemicals*, Aldrich Chemical Company, Inc., Milwaukee WI, 1990, vol. 1.
78 Y. Opata and J.-C. Grivel, *J. Anal. Appl. Pyrolysis*, 2018, **132**, 40.
79 H. Eloussifi, J. Farjas, P. Roura, J. Camps, M. Dammak, S. Ricart, T. Puig and X. Obradors, *J. Therm. Anal. Calorim.*, 2012, **108**, 589.
80 K. Krämer, D. Biner, G. Frei, H. Güdel, M. Hehlen and S. Lüthi, *Chem. Mater.*, 2004, **16**, 1244.